NANO LETTERS

Letter

pubs.acs.org/NanoLett

Blue-Green Color Tunable Solution Processable Organolead Chloride–Bromide Mixed Halide Perovskites for Optoelectronic Applications

Aditya Sadhanala,*[,†] Shahab Ahmad,[‡] Baodan Zhao,[†] Nadja Giesbrecht,[§] Phoebe M. Pearce,[†] Felix Deschler,[†] Robert L. Z. Hoye,[†] Karl C. Gödel,[†] Thomas Bein,[§] Pablo Docampo,[§] Siân E. Dutton,[†] Michael F. L. De Volder,[‡] and Richard H. Friend*[,†]

[†]Cavendish Laboratory, JJ Thomson Avenue, CB3 0HE, Cambridge, United Kingdom

[‡]Department of Engineering, Cambridge University, 17 Charles Babbage Road, CB3 0FS, Cambridge, United Kingdom

[§]Department of Chemistry and Center for NanoScience, Ludwig-Maximilians-Universität München, Butenandtstraße 5-13, 81377 München, Germany

Supporting Information

ABSTRACT: Solution-processed organo-lead halide perovskites are produced with sharp, color-pure electroluminescence that can be tuned from blue to green region of visible spectrum (425–570 nm). This was accomplished by controlling the halide composition of $CH_3NH_3Pb(Br_xCl_{1-x})_3$ $[0 \le x \le 1]$ perovskites. The bandgap and lattice parameters change monotonically with composition. The films possess remarkably sharp band edges and a clean bandgap, with a single optically active phase. These chloride–bromide perovskites can potentially be used in optoelectronic devices like solar cells and light emitting diodes (LEDs). Here we demonstrate high color-purity, tunable LEDs with narrow emission full width at half maxima (FWHM) and low turn on voltages using thin-films of these perovskite materials, including a blue $CH_3NH_3PbCl_3$ perovskite LED with a narrow emission FWHM of 5 nm.

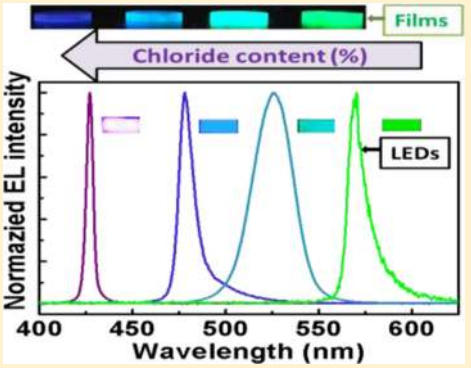

KEYWORDS: *Blue perovskite LED, chloride bromide perovskite, narrow FWHM, disorder, bandgap tuning*

The field of solution processed organic–inorganic halide perovskite based optoelectronics has emerged in the last couple of years.[1−6] This was initially driven by solar cells based on organo-lead halide perovskite that now demonstrate power conversion efficiencies of above 20%.[7] Thin films based on the mixed-halide $CH_3NH_3Pb(I_xCl_{1-x})_3$ version of these perovskite materials also feature high photoluminescence quantum yield (PLQE).[8] The demonstration of these high radiative emission efficiencies led to the development of bright light emitting diodes (LEDs) and optically pumped lasers.[5,8,9] There are recent reports that the optical bandgap of lead halide perovskites can be tuned in the visible range of ∼550–780 nm through the use of solid solutions of bromide-iodide mixed halides.[10−12] These solid solution based thin films can be easily prepared by varying the ratio of the two individual pure trihalide perovskite solutions mixed together (for example, $CH_3NH_3PbI_3$ and $CH_3NH_3PbBr_3$). However, tuning the bandgap in the blue–green region using solution processed chloride–bromide mixed halide perovskites has been a challenging task, given the low solubility of the chloride containing precursor materials (CH_3NH_3Cl and $PbCl_2$) in regularly used solvents like *N*,*N*-dimethylformamide (DMF). We here make use of mixed solvents DMF and dimethyl sulfoxide (DMSO) along with an organic lead source of lead acetate $Pb(CH_3COO)_2$ to achieve the solution processability of the chloride containing precursor materials. Realizing such large bandgap solution processed semiconductors is of great importance given their utility in making tandem solar cells and making LEDs which emit in the blue-green range of the visible spectrum.

Here, we demonstrate bandgap tuning of the $CH_3NH_3Pb(Br_xCl_{1-x})_3$ $[0 \le x \le 1]$ perovskites in the UV–visible (UV–vis) range of ∼3.1–2.3 eV. We tuned the bandgap in this range by varying the chloride to bromide ratios in the $CH_3NH_3Pb(Br_xCl_{1-x})_3$ $[0 \le x \le 1]$ perovskites, which are solution processed from their respective precursor solutions. These solution processed mixed chloride–bromide films were further characterized using X-ray diffraction (XRD), photothermal deflection spectroscopy (PDS), time-resolved photoluminescence (TRPL), and energy dispersive X-ray (EDX) measurements. These mixed chloride–bromide perovskites provide a way to realize solution processed large bandgap perovskite solar cells to combine with small bandgap perovskite solar cells in tandem architecture. Furthermore, these perovskites allow blue

Received: June 15, 2015
Revised: July 22, 2015
Published: August 3, 2015

DOI: 10.1021/acs.nanolett.5b02369
Nano Lett. 2015, 15, 6095–6101

LEDs to be realized, which have proven to be a difficult task with gallium nitride (GaN) being the only widely used option for commercial application. We here demonstrate the use of the $CH_3NH_3Pb(Br_xCl_{1-x})_3$ perovskites in the fabrication of LEDs with color tunability dependent on the composition, and for $CH_3NH_3Pb(Br_xCl_{1-x})_3$ $[x < 0.6]$ we demonstrate blue LEDs with narrow emission full-width at half maxima (FWHM).

Bandgap tuning in the $CH_3NH_3Pb(Br_xCl_{1-x})_3$ $[0 \le x \le 1]$ perovskites was achieved by substitution of Br and Cl ions in the precursor solutions. We prepared perovskite precursor solutions with two different organic (CH_3NH_3X) to inorganic ($Pb(CH_3COO)_2$) molar ratios—3:1 and 5:1 organic to inorganic (for detailed description of material preparation refer to the Supporting Information). We note that these ratios correspond respectively to (1) a stoichiometric solution and (2) one with an excess of CH_3NH_3X, and these are analogous to the 1:1 and 3:1 ratios for methylammonium halide and lead halide starting materials typically used.[5,13,14] The photophysical properties of the 3:1 molar starting ratio perovskite samples are summarized in the Supporting Information (Figures S1, S2, and S3). In brief, we observe a monotonic blue shift in the bandgap with decreasing bromide content and increasing chloride content in the $CH_3NH_3Pb(Br_xCl_{1-x})_3$ $[0 \le x \le 1]$ perovskites. X-ray diffraction of the $CH_3NH_3Pb(Br_xCl_{1-x})_3$ films formed using the stoichiometric solution indicates formation of a cubic perovskite, space group *Pm3m*, across the entire composition range $[0 \le x \le 1]$. In agreement with Vegard's law, a monotonic decrease in the lattice parameter with increasing chloride content is observed. These 3:1 molar staring ratio perovskite materials could be useful in solar cell applications as their band-edges are sharper with clean sub-bandgap and narrow XRD diffraction peaks (see Supporting Information, Figures S1, S2, and S3 for PDS and XRD spectra). However, for luminescence applications, we use 5:1 organic to inorganic molar starting ratio perovskite materials analogous to the materials used to make efficient perovskite LEDs previously,[5,14−17] and these are described in detail as follows.

EDX measurements were performed (see Supporting Information, Figure S4) to determine the nominal halide composition in the 5:1 organic-to-inorganic molar starting ratio based $CH_3NH_3Pb(Br_xCl_{1-x})_3$ $[0 \le x \le 1]$ perovskite films spin-coated onto quartz substrates, and it was found that the halide content in films is similar to that in the precursor mixture solutions within the detection error limits of the measurement (±5%). Henceforth, the composition indicated in rest of the manuscript is that of the respective perovskite films.

The optical properties of 5:1 organic-to-inorganic molar starting ratio based $CH_3NH_3Pb(Br_xCl_{1-x})_3$ $[0 \le x \le 1]$ perovskite films spin-coated onto quartz substrates were measured. The absorption spectra in Figure 1a show a monotonic blue shift in the bandgap of these films with decreasing bromide content (or increasing chloride content), from a band-edge of around 530 nm for 0% chloride sample ($CH_3NH_3PbBr_3$) to 400 nm for the 100% chloride sample ($CH_3NH_3PbCl_3$). To analyze the quality of semiconductor formed, we performed PDS measurements to probe the sub-bandgap absorption of our perovskite films. PDS is a highly sensitive absorption measurement technique capable of measuring absorbances down to 10^{-5} and is not subject to optical effects, such as light scattering, reflection, and interference effects at the substrate/material interface. PDS has been extensively used to study various organo-metal halide perovskites to measure the sub-bandgap defect states,

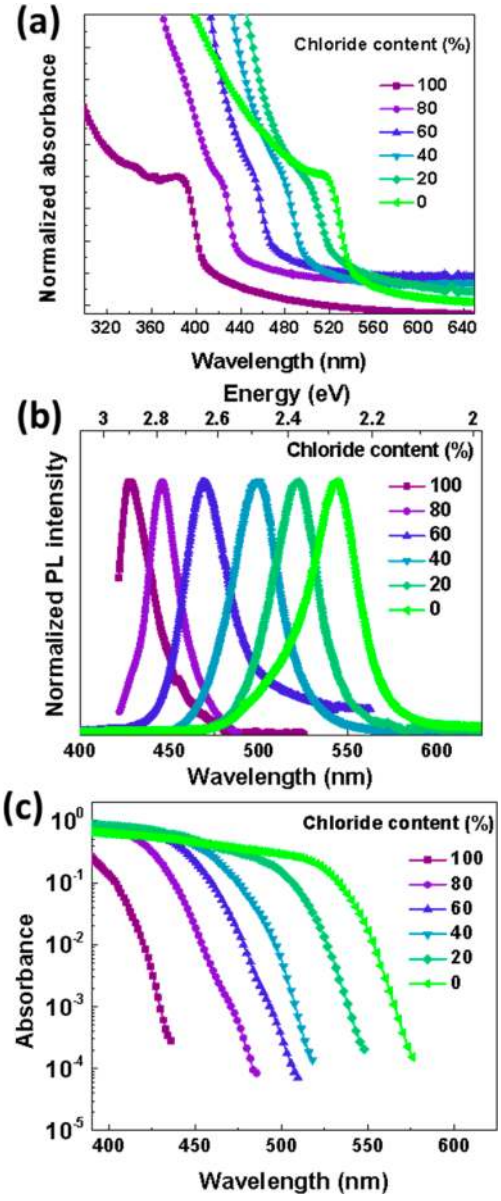

Figure 1. (a) UV−visible absorption spectra and (b) normalized photoluminescence spectra for the 5:1 organic to inorganic molar starting ratio $CH_3NH_3Pb(Br_xCl_{1-x})_3$ $[0 \le x \le 1]$ perovskite thin films with different chloride−bromide ratios as indicated. Excitation for PL was performed with a pulsed laser system at 3.1 eV photon energy and 100 fs pulse length, and PL spectra have been normalized to the peak emission. (c) PDS spectra showing sharp band edges and a clean bandgap.

degradation, and energetic disorder in the form of Urbach energy.[5,12,13,18−20] The PDS spectra for the 5:1 organic to inorganic molar starting ratio $CH_3NH_3Pb(Br_xCl_{1-x})_3$ $[0 \le x \le 1]$ perovskite films is shown in Figure 1c, which shows a blue shift in the bandgap with increasing chloride content in the perovskite films. We find that all of these perovskite films have sharp band edges and clean sub-bandgap absorption indicating the superior quality of the semiconductor formed. Steady-state PL spectra of the 5:1 organic to inorganic molar starting ratio $CH_3NH_3Pb(Br_xCl_{1-x})_3$ $[0 \le x \le 1]$ perovskites were measured (Figure 1b). We observe a systematic blue shift in the PL spectra with increasing chloride content from 543 nm for 0% chloride perovskite ($CH_3NH_3PbBr_3$) to 428 nm for 100%

DOI: 10.1021/acs.nanolett.5b02369
Nano Lett. 2015, 15, 6095−6101

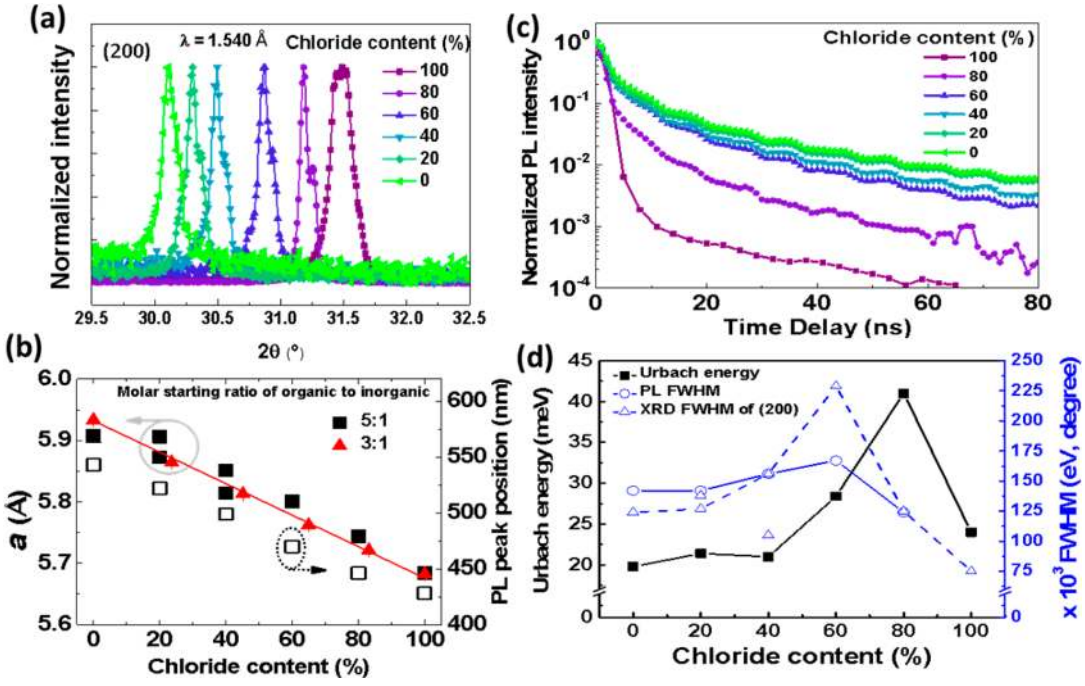

Figure 2. (a) XRD patterns showing the evolution of the (200) reflection as a function of composition for 5:1 molar starting ratio $CH_3NH_3Pb(Br_xCl_{1-x})_3$ $[0 \le x \le 1]$ perovskite thin films showing diffraction pattern shift to higher scattering angle, 2θ with increasing chloride content. (b) Changes of normalized lattice parameters for 5:1 (closed squares) and 3:1 (closed triangles) organic-to-inorganic molar starting ratio $CH_3NH_3Pb(Br_xCl_{1-x})_3$ $[0 \le x \le 1]$ perovskite thin films and PL peak position with change in composition for the same films. (c) Plot of normalized PL intensity versus time for same films. (d) Comparison of the change in FWHM of the PL emission peak, (200) XRD reflection, and the Urbach energy calculated from PDS measurements for the same films. The normalized lattice parameter and XRD FWHM show two data points for 20% and 40% chloride samples each, and these values are for the split phases observed in the XRD of these samples. Excitation for PL was performed with a pulsed laser system at 3.1 eV photon energy and 100 fs pulse length.

chloride perovskite ($CH_3NH_3PbCl_3$). The PL and the PDS spectra demonstrate that the resulting $CH_3NH_3Pb(Br_xCl_{1-x})_3$ $[0 \le x \le 1]$ perovskite films demonstrate a single optically active phase. This finding supports our observation of a clean bandgap in these films.

XRD studies of the $CH_3NH_3Pb(Br_xCl_{1-x})_3$ $[0 \le x \le 1]$ perovskite films formed using the 5:1 molar starting ratio solutions (Figure 2a), indicate the formation of a cubic phase, space group *Pm3m*, across the composition range (for full XRD spectra see Supporting Information, Figure S5). Quantitative analysis to determine the lattice parameters was carried out using a Le Bail analysis,[21] in the Fullprof suite of programmes;[22] preferential alignment in the films prevents a full analysis of the crystal structure. As the chloride content increases, the peaks in the diffraction pattern shift to higher scattering angle, 2θ, as would be expected when bromide is replaced by smaller chloride ions. At low chloride concentrations (20−40% Cl) the high angle peaks at 30−31.5° 2θ (Figure 2a) are observed to split, indicating the formation of cubic perovskites with more than one lattice parameter. Given the monotonic variation in the lattice parameters in the 3:1 films with composition, this is most likely to arise as a result of bulk phase segregation into perovskite crystals with different ratios of halides with composition within 10% of the initial starting solution. From the current analysis, it is not possible to determine the relative phase fraction of the perovskites formed and so it is not possible to quantify the extent of the phase segregation. At higher chloride concentrations ($x > 0.4$) a single perovskite phase is seen in the XRD patterns; however, the broadening of the reflections may indicate some less extensive phase segregation.

In Figure 2b, we compare the change in the PL peak positions alongside the extracted normalized lattice parameters, where both follow a linear trend with the changing chloride fraction for the 5:1 organic to inorganic molar starting ratio $CH_3NH_3Pb(Br_xCl_{1-x})_3$ $[0 \le x \le 1]$ perovskite films. We further measured the photoluminescence kinetics of the 5:1 organic to inorganic molar starting ratio $CH_3NH_3Pb(Br_xCl_{1-x})_3$ $[0 \le x \le 1]$ perovskite films (Figure 2c) which show single bimolecular decays for the 0% chloride film ($CH_3NH_3PbBr_3$) and also for films down to 60% chloride sample, similar to what was reported previously for bromide−iodide mixed halide perovskite materials.[8,12] Films with 80% and 100% chloride content both show faster kinetics than the films with lower chloride content.

The Urbach energies were measured for all of the 5:1 organic to inorganic molar starting ratio $CH_3NH_3Pb(Br_xCl_{1-x})_3$ $[0 \le x \le 1]$ perovskite films using the PDS spectra. Urbach energy "E_U" is an empirical parameter that gives an indication of the energetic disorder for a given semiconductor.[23,24] The Urbach energy is derived from the PDS absorption data by using the following expression: $A = A_0 \exp((E - E_g)/E_U)$, where A is the absorbance, A_0 is a constant, and E_g is the bandgap of the material.[12,24,25] Figure 2d shows the correlation between the extracted Urbach energies and the full width at half maxima (FWHM) of the PL spectra and the (200) XRD reflection of the 5:1 organic to inorganic molar starting ratio $CH_3NH_3Pb(Br_xCl_{1-x})_3$ $[0 \le x \le 1]$ perovskite films with various chloride content. It can be seen that the Urbach energy is the lowest for the 0% chloride ($CH_3NH_3PbBr_3$) sample at 20 meV and increases monotonically with increasing chloride content to 41 meV for the 80% chloride film and then drops down to 31 meV

DOI: 10.1021/acs.nanolett.5b02369
Nano Lett. 2015, 15, 6095−6101

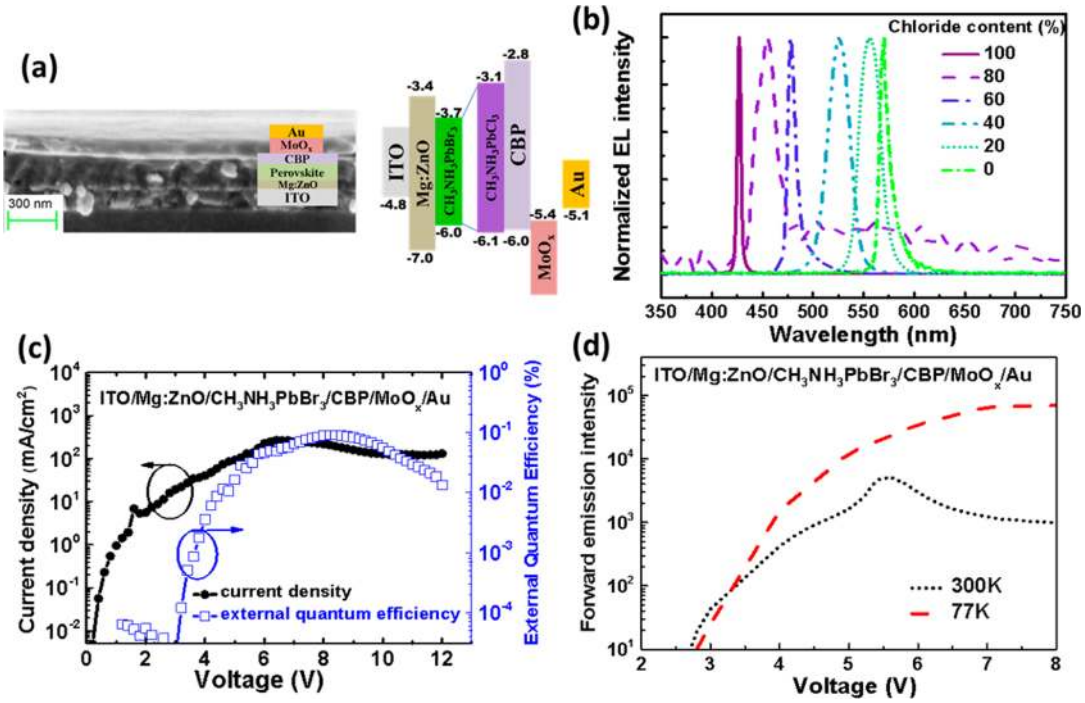

Figure 3. (a) Device structure of the perovskite LEDs. (b) Normalized EL spectra of the 5:1 organic to inorganic molar starting ratio $CH_3NH_3Pb(Br_xCl_{1-x})_3$ $[0 \leq x \leq 1]$ perovskite thin film based LEDs with different chloride−bromide ratios as indicated and measured at 77 K. These LEDs were fabricated in a device structure comprising of ITO/Mg:ZnO/perovskite/CBP/MoO_x/Au and they demonstrate high color purity and emission tunability with change in composition. (c) Current density and external quantum efficiency curves for the 0% chloride ($CH_3NH_3PbBr_3$) LED measured at room temperature (300 K) and (d) the forward emission of this LED with respect to bias voltage for the same device at room (300 K) and liquid nitrogen (77 K) temperatures.

for the 100% chloride sample ($CH_3NH_3PbCl_3$). We also observe a similar trend in the PL with a minimum for the 0% chloride ($CH_3NH_3PbBr_3$) and 80% chloride ($CH_3NH_3Pb(Br_{0.2}Cl_{0.8})_3$) samples at 142 and 124 meV, respectively. Furthermore, the PL FWHM increases monotonically with increasing chloride content in the films to reach a maximum of 167 meV for 60% chloride sample ($CH_3NH_3Pb(Br_{0.4}Cl_{0.6})_3$). The FWHM of a process (absorption and emission) is generally indicative of the magnitude of disorder experienced by the excited carriers in the energetic landscape around them. Interestingly, the FWHM of the (200) reflection XRD shows similar trend as the PL FWHM and Urbach energy. This similarity in the trends between Urbach energy, PL FWHM and XRD FWHM, indicates the possibility that the energetic disorder experienced by the absorptive and emissive species are similar and are related to the structural disorder.

In order to demonstrate the potential application of these $CH_3NH_3Pb(Br_xCl_{1-x})_3$ $[0 \leq x \leq 1]$ perovskite films in optoelectronic devices, we fabricated light-emitting diodes using these 5:1 organic to inorganic molar starting ratio $CH_3NH_3Pb(Br_xCl_{1-x})_3$ $[0 \leq x \leq 1]$ perovskite films. The device structure used in this work is ITO/Mg:ZnO/$CH_3NH_3Pb(Br_xCl_{1-x})_3$/CBP/$MoO_x$/Au, where a combination of indium tin oxide (ITO) coated glass substrate and 50 nm ZnO followed by 10 nm zinc magnesium oxide (Mg:ZnO) forms the electron selective contact and the combination of 25 nm 4,4′-Bis(*N*-carbazolyl)-1,1′-biphenyl (CBP), 15 nm molybdenum trioxide, and 100 nm gold (Au) electrode act as a hole-selective contact. This device structure is depicted in Figure 3a along with the energy levels. The energy levels of the perovskite films were measured using Ultraviolet photoelectron spectroscopy (UPS) (see Supporting Information, Figure S6) and all other energy levels were obtained from various literature reports.[26,27] We measured the electroluminescence (EL) spectra for devices with varying chloride content, $CH_3NH_3Pb(Br_xCl_{1-x})_3$ $[0 \leq x \leq 1]$ (Figure 3b). At room temperature weak or no EL could be measured except for the 0% chloride ($CH_3NH_3PbBr_3$) based perovskite LED device which gave us a peak external quantum efficiency (EQE) of around 0.1% at ∼6 V which is comparable to previous reports.[5,28] This LED demonstrated a near bandgap turn on at around 2.2 V indicating efficient and balanced charge injection in the device. The other LEDs containing different chloride content other than 0% chloride did not show weak or no measurable EL emission at room temperature. However, on cooling below 200 K, EL is observed in devices containing the mixed halide, 5:1 organic to inorganic molar starting ratio $CH_3NH_3Pb(Br_xCl_{1-x})_3$ $[0 \leq x < 1]$, perovskite films. The EQE could not be measured at low temperatures due to experimental difficulties. Nevertheless, we compare the peak forward emission intensity of the 100% bromide ($CH_3NH_3PbBr_3$) device at room temperature and 77 K (Figure 3b) which is indicative of the device performance at the measured temperatures. From Figure 3c and d, we observe that the turn on voltage remains at 2.2−3 V even at 77 K—similar to what we observe at room temperature. This is an interesting observation given the device turn on voltages for conventional organic LEDs (OLEDs) increases with decreases in temperature.[29] The forward emission intensity of this device also increases at low temperatures, indicating the improvement in the photoluminescence quantum efficiency (PLQE) at low temperatures due to a potential reduction in nonradiative recombination pathways at low temperatures.[30]

DOI: 10.1021/acs.nanolett.5b02369
Nano Lett. 2015, 15, 6095−6101

In Figure 3b we demonstrate the ability to tune the bandgap and emission wavelength of the LEDs based on the mixed halide, 5:1 organic-to-inorganic molar starting ratio $CH_3NH_3Pb(Br_xCl_{1-x})_3$ $[0 \leq x < 1]$, perovskite films which were measured at liquid nitrogen temperatures (77 K). The EL emission wavelength monotonically changes from 570 nm for 0% chloride ($CH_3NH_3PbBr_3$) based LED to 427 nm for the 100% chloride LED ($CH_3NH_3PbCl_3$). One notable observation is the narrow 5 nm EL FWHM for the 100% chloride ($CH_3NH_3PbCl_3$) perovskite based LED, which to our knowledge is one of the lowest FWHM observed to date for any solution processed material.[5,14,17,28,31]

The reason for the materials with large bandgap not showing any EL at room temperature could probably be the optical instability of these perovskite films. Recently, it was reported that the mixed halide bromide-iodide perovskite show optical instability under solar illumination (100 mW/cm^2).[32] To rule out any such optical instability in these perovskites, we performed PL measurements on the 60% chloride ($CH_3NH_3Pb(Br_{0.4}Cl_{0.6})_3$) sample before and immediately after a 10 min exposure under 1 sun illumination (100 mW/cm^2) (see Supporting Information, Figure S9). We found that the PL peak position does not change before and after illumination, which suggests that these 5:1 organic-to-inorganic molar starting ratio $CH_3NH_3Pb(Br_xCl_{1-x})_3$ $[0 \leq x < 1]$ perovskite films are optically stable. One other reason behind the lack of EL at room temperature from the LEDs fabricated using large bandgap perovskite films could be the low PLQE. We investigates this by measuring the integrated PL from the 60% chloride ($CH_3NH_3Pb(Br_{0.4}Cl_{0.6})_3$) perovskite film at low temperatures. The integrated PL from this film increases with decrease in temperature from room temperature (300 K) down to liquid nitrogen temperature (77 K). This can be inferred as an increase in PLQE at low temperatures, and this can be further inferred from the PL activation curve (see Supporting Information, Figure S10). We observe an increase in the integrated PL intensity for the 60% chloride sample with decreasing temperature indicating the presence of efficient nonradiative processes at room temperature which are suppressed on cooling.[30] We estimate activation energies in the range of ∼590 meV for this thermally activated PL quenching.

Nevertheless, the fact that the LEDs based on these perovskite materials demonstrate narrow emission and low turn on voltages at low temperatures along with the color tunability is a step forward to realize high color purity tunable LEDs. Further investigation into increasing the quality and PLQE of perovskite materials can help us realize blue LEDs operating at room temperature, and this could become a potential alternative to the current industrial standard—gallium nitride (GaN) based blue LEDs.

In summary, we demonstrate bandgap tuning in the green to blue region of the visible spectrum using solution-processed $CH_3NH_3Pb(Br_xCl_{1-x})_3$ $[0 \leq x < 1]$ perovskites. We overcame the challenge of incorporating chloride into perovskite structures containing bromide by using mixed solvent approach and organic source of lead. These color tunable materials have been used to fabricate high color-purity, tunable LEDs with narrow FWHM emission and low turn on voltages. With further investigation into increasing the quality of mixed chloride−bromide perovskites, $CH_3NH_3Pb(Br_xCl_{1-x})_3$, to enhance the PLQE, these materials may offer an alternative to current gallium nitride (GaN) based blue LED technologies.

Experimental Section. *Perovskite Precursor Mixture Solution Preparation. 3:1 Molar Starting Ratio Precursor Mixture Solutions.* $CH_3NH_3PbBr_3$ precursor solution was synthesized by mixing CH_3NH_3Br and $Pb(CH_3COO)_2$ in a 3:1 molar stoichiometric ratio in DMF to obtain a 0.5 M solution. Similarly, the $CH_3NH_3PbCl_3$ precursor solution was synthesized by mixing CH_3NH_3Cl and $Pb(CH_3COO)_2$ in a 3:1 molar stoichiometric ratio in a mixed solvent comprising DMSO and DMF in the ratio of 40:60 (v/v) to get a 0.5 M solution. To prepare the desired $CH_3NH_3Pb(Br_xCl_{1-x})_3$ $[0 \leq x \leq 1]$ precursor solutions, the above-mentioned $CH_3NH_3PbBr_3$ and $CH_3NH_3PbCl_3$ precursor solutions were mixed together in the required stoichiometric ratios.

5:1 Organic-to-Inorganic Molar Starting Ratio Precursor Mixture Solutions. $CH_3NH_3PbBr_3$ precursor solution was synthesized by mixing CH_3NH_3Br and $Pb(CH_3COO)_2$ in a 5:1 molar stoichiometric ratio in DMF to obtain a 0.5 M solution. Similarly, the $CH_3NH_3PbCl_3$ precursor solution was synthesized by mixing CH_3NH_3Cl and $Pb(CH_3COO)_2$ in a 5:1 molar stoichiometric ratio in a mixed solvent comprising DMSO and DMF in the ratio of 40:60 (v/v) to get a 0.5 M solution. To prepare the desired $CH_3NH_3Pb(Br_xCl_{1-x})_3$ $[0 \leq x \leq 1]$ precursor solutions, the above-mentioned $CH_3NH_3PbBr_3$ and $CH_3NH_3PbCl_3$ precursor solutions were mixed together in the required stoichiometric ratios.

Device Fabrication. Prepatterned ITO substrates were cleaned using ultrasonic bath in acetone followed by isopropanol for 15 min each. The cleaned substrates were subjected to oxygen plasma cleaning for 1 min. The magnesium-doped zinc oxide films (ZnO:Mg) were deposited at 150 °C using an atmospheric pressure spatial atomic layer deposition (AP-SALD) reactor operating in chemical vapor deposition (CVD) conditions.[33] First, 50 nm of ZnO was deposited onto these substrates, followed by 10 nm of $Zn_{0.56}Mg_{0.44}O$ on top. We used previously reported flow conditions for these depositions.[17] After deposition, the films were cleaned by soaking in acetone for 1 h, followed by 3 min of sonication in ethanol. All films were annealed at 400 °C for 15 min in air. Further, a 5 nm PEI layer was deposited using a 0.4 wt % solution in 2-methoxyethanol followed by annealing for 10 min at 100 °C. Desired perovskite precursor mixture solutions were spin-coated and annealed in nitrogen filled glovebox at 100 °C for 5 min. The resulting thickness of the perovskite film was in the range of 125−150 nm. We then spin-coated a 25 nm thin layer of CBP from a chlorobenzene solution. This was followed by thermal evaporation of 15 nm of MoO_x and 100 nm of gold which forms the top electrode.

LED Characterization. Current−voltage (I−V) characteristics were measured using a Keithley 2400 source measure unit. The photon flux emitted during the scan was measured using a calibrated silicon photodetector, and the external quantum efficiency (EQE) was calculated assuming a Lambertian emission profile. The electroluminescence spectra were measured using an optical fiber connected to a calibrated Ocean Optics USB 2000+ spectrometer. A Oxford instruments flow cryostat was used to perform the LED measurements at low temperature with liquid helium as a cooling medium. At low temperatures, the LED was driven by manually changing the device bias and by coupling the EL output into an a gated intensified CCD camera system (Andor iStar DH740 CCI-010) connected to a grating spectrometer (Andor SR303i).

Photoluminescence and Lifetime Measurements. Time-resolved photoluminescence measurements were taken with a

DOI: 10.1021/acs.nanolett.5b02369
Nano Lett. 2015, 15, 6095−6101

gated intensified CCD camera system (Andor iStar DH740 CCI-010) connected to a grating spectrometer (Andor SR303i). Excitation was performed with femtosecond laser pulses which were generated by in a home-built setup by second order generation (SHG) in a BBO crystal form the fundamental output (pulse energy 1.55 eV, pulse length 50 fs) of a Ti:sapphire laser system (Spectra Physics Soltstice). The laser pulses generated from the SHG had photon energy of 3.1 eV, pulse length ~100 fs.

Absorption Measurement. Linear absorption spectra of thin-films deposited on quartz substrates were measured using Hewlett-Packard 8453 UV−vis spectrometer with blank substrate correction.

Photothermal deflection spectroscopy (PDS) technique was used for the absorption measurements. Films spun on quartz substrates were used for the measurements. PDS is a highly sensitive scatter-free surface averaged absorption measurement technique capable of measuring absorbances down to 10^{-5}. A detailed description about the PDS setup can be found in Sadhanala et al.[12]

Details of XRD Measurements. X-ray diffraction measurements were made on thin film samples of $CH_3NH_3Pb(Br_xCl_{1-x})_3$ $[0 \leq x \leq 1]$, on a Bruker D8 discover diffractometer with Cu Kα radiation, λ = 1.5403 Å. Samples were measured using a Bragg−Brentano geometry over $10 \leq 2\theta \leq 60°$ with a step size of $\Delta 2\theta = 0.01°$. Due to preferential alignment in the films, a complete structural analysis was not possible. Instead, the symmetry and lattice parameters were modeled using a Le Bail analysis in the Fullprof suite of programmes. Backgrounds fit were using a refined interpolation of points, and the peak shape was modeled using a pseudo-Voigt function.

■ ASSOCIATED CONTENT

Supporting Information

The Supporting Information is available free of charge on the ACS Publications website at DOI: 10.1021/acs.nanolett.5b02369.

Additional figures, including EDX, PDS absorption spectra, XRD spectra, and SEM images (PDF)

■ AUTHOR INFORMATION

Corresponding Authors

*E-mail: as2233@cam.ac.uk.
*E-mail: rhf10@cam.ac.uk.

Present Address

R.L.Z.H.: Photovoltaic Research Laboratory, Massachusetts Institute of Technology, Cambridge, Massachusetts 02139, USA.

Notes

The authors declare no competing financial interest.

■ ACKNOWLEDGMENTS

We acknowledge funding from the Engineering and Physical Sciences Research Council (EPSRC) and the Winton Programme (Cambridge) for the Physics of Sustainability. Support from the Deutsche Forschungsgemeinschaft (NIM Excellence Cluster) is gratefully acknowledged. A.S. acknowledges the funding and support from the Indo-UK APEX project. F.D. acknowledges funding and support from a Herchel Smith fellowship. M.D.V. acknowledges funding and support from the ERC-StG 337739-HIENA. A.S. thanks Dr. D. Di for the insightful discussions. P. D. gratefully acknowledges support from the European Union in the form of a Marie Curie Intra-European fellowship.

■ REFERENCES

(1) Lee, M. M.; Teuscher, J.; Miyasaka, T.; Murakami, T. N.; Snaith, H. J. Efficient Hybrid Solar Cells Based on Meso-Superstructured Organometal Halide Perovskites. *Science* **2012**, *338*, 643−647.

(2) Kim, H.-S.; Lee, C.-R.; Im, J.-H.; Lee, K.-B.; Moehl, T.; Marchioro, A.; Moon, S.-J.; Humphry-Baker, R.; Yum, J.-H.; Moser, J. E.; et al. Lead Iodide Perovskite Sensitized All-Solid-State Submicron Thin Film Mesoscopic Solar Cell with Efficiency Exceeding 9%. *Sci. Rep.* **2012**, *2*, 591−598.

(3) Luo, J.; Im, J.-H.; Mayer, M. T.; Schreier, M.; Nazeeruddin, M. K.; Park, N.-G.; Tilley, S. D.; Fan, H. J.; Gratzel, M. Water Photolysis at 12.3% Efficiency via Perovskite Photovoltaics and Earth-Abundant Catalysts. *Science* **2014**, *345*, 1593−1596.

(4) Zhou, H.; Chen, Q.; Li, G.; Luo, S.; Song, T.; Duan, H.-S.; Hong, Z.; You, J.; Liu, Y.; Yang, Y. Photovoltaics. Interface Engineering of Highly Efficient Perovskite Solar Cells. *Science* **2014**, *345*, 542−546.

(5) Tan, Z.-K.; Moghaddam, R. S.; Lai, M. L.; Docampo, P.; Higler, R.; Deschler, F.; Price, M.; Sadhanala, A.; Pazos, L. M.; Credgington, D.; et al. Bright Light-Emitting Diodes Based on Organometal Halide Perovskite. *Nat. Nanotechnol.* **2014**, *9*, 687−692.

(6) Green, M. A.; Ho-Baillie, A.; Snaith, H. J. The Emergence of Perovskite Solar Cells. *Nat. Photonics* **2014**, *8*, 506−514.

(7) Yang, W. S.; Noh, J. H.; Jeon, N. J.; Kim, Y. C.; Ryu, S.; Seo, J. High-Performance Photovoltaic Perovskite Layers Fabricated through Intramolecular Exchange. *Science* **2015**, *348*, 1234−1237.

(8) Deschler, F.; Price, M.; Pathak, S.; Klintberg, L. E.; Jarausch, D.-D.; Higler, R.; Hüttner, S.; Leijtens, T.; Stranks, S. D.; Snaith, H. J.; et al. High Photoluminescence Efficiency and Optically Pumped Lasing in Solution-Processed Mixed Halide Perovskite Semiconductors. *J. Phys. Chem. Lett.* **2014**, *5*, 1421−1426.

(9) Xing, G.; Mathews, N.; Lim, S. S.; Yantara, N.; Liu, X.; Sabba, D.; Grätzel, M.; Mhaisalkar, S.; Sum, T. C. Low-Temperature Solution-Processed Wavelength-Tunable Perovskites for Lasing. *Nat. Mater.* **2014**, *13*, 476−480.

(10) Noh, J. H.; Im, S. H.; Heo, J. H.; Mandal, T. N.; Seok, S. Il. Chemical Management for Colorful, Efficient, and Stable Inorganic-Organic Hybrid Nanostructured Solar Cells. *Nano Lett.* **2013**, *13*, 1764−1769.

(11) Eperon, G. E.; Stranks, S. D.; Menelaou, C.; Johnston, M. B.; Herz, L. M.; Snaith, H. J. Formamidinium Lead Trihalide: A Broadly Tunable Perovskite for Efficient Planar Heterojunction Solar Cells. *Energy Environ. Sci.* **2014**, *7*, 982−988.

(12) Sadhanala, A.; Deschler, F.; Thomas, T. H.; Dutton, S. E.; Goedel, K. C.; Hanusch, F. C.; Lai, M. L.; Steiner, U.; Bein, T.; Docampo, P.; et al. Preparation of Single-Phase Films of $CH_3NH_3Pb(I_{1-X}Br_X)_3$ with Sharp Optical Band Edges. *J. Phys. Chem. Lett.* **2014**, *5*, 2501−2505.

(13) Zhang, W.; Saliba, M.; Moore, D. T.; Pathak, S. K.; Hörantner, M. T.; Stergiopoulos, T.; Stranks, S. D.; Eperon, G. E.; Alexander-Webber, J. A.; Abate, A.; et al. Ultrasmooth Organic−inorganic Perovskite Thin-Film Formation and Crystallization for Efficient Planar Heterojunction Solar Cells. *Nat. Commun.* **2015**, *6*, 6142.

(14) Wang, J.; Wang, N.; Jin, Y.; Si, J.; Tan, Z.-K.; Du, H.; Cheng, L.; Dai, X.; Bai, S.; He, H.; et al. Interfacial Control Toward Efficient and Low-Voltage Perovskite Light-Emitting Diodes. *Adv. Mater.* **2015**, *27*, 2311−2316.

(15) Li, G.; Tan, Z.-K.; Di, D.; Lai, M. L.; Jiang, L.; Lim, J. H.; Friend, R. H.; Greenham, N. C. Efficient Light-Emitting Diodes Based on Nanocrystalline Perovskite in a Dielectric Polymer Matrix. *Nano Lett.* **2015**, *15*, 2640−2644.

(16) Kumawat, N. K.; Dey, A.; Narasimhan, K. L.; Kabra, D. Near Infrared to Visible Electroluminescent Diodes Based on Organometallic Halide Perovskites: Structural and Optical Investigation. *ACS Photonics* **2015**, *2*, 349−354.

DOI: 10.1021/acs.nanolett.5b02369
Nano Lett. 2015, 15, 6095−6101

(17) Hoye, R. L. Z.; Chua, M. R.; Musselman, K. P.; Li, G.; Lai, M.-L.; Tan, Z.-K.; Greenham, N. C.; MacManus-Driscoll, J. L.; Friend, R. H.; Credgington, D. Enhanced Performance in Fluorene-Free Organometal Halide Perovskite Light-Emitting Diodes Using Tunable, Low Electron Affinity Oxide Electron Injectors. *Adv. Mater.* **2015**, *27*, 1414−1419.
(18) Noel, N. K.; Stranks, S. D.; Abate, A.; Wehrenfennig, C.; Guarnera, S.; Haghighirad, A.; Sadhanala, A.; Eperon, G. E.; Pathak, S. K.; Johnston, M. B.; et al. Lead-Free Organic-Inorganic Tin Halide Perovskites for Photovoltaic Applications. *Energy Environ. Sci.* **2014**, *7*, 3061−3068.
(19) Di, D.; Musselman, K. P.; Li, G.; Sadhanala, A.; Ievskaya, Y.; Song, Q.; Tan, Z.-K.; Lai, M. L.; MacManus-Driscoll, J. L.; Greenham, N. C.; et al. Size-Dependent Photon Emission from Organometal Halide Perovskite Nanocrystals Embedded in an Organic Matrix. *J. Phys. Chem. Lett.* **2015**, *6*, 446−450.
(20) Sadhanala, A.; Kumar, A.; Pathak, S.; Rao, A.; Steiner, U.; Greenham, N. C.; Snaith, H. J.; Friend, R. H. Electroluminescence from Organometallic Lead Halide Perovskite-Conjugated Polymer Diodes. *Adv. Electron. Mater.* **2015**, *1*, 1500008.
(21) Le Bail, A.; Duroy, H.; Fourquet, J. L. Ab-Initio Structure Determination of $LiSbWO_6$ by X-Ray Powder Diffraction. *Mater. Res. Bull.* **1988**, *23*, 447−452.
(22) Rodriguez-Carvajal, J.; Fernandez-Diaz, M. T.; Martinez, J. L. Neutron Diffraction Study on Structural and Magnetic Properties of La_2NiO_4. *J. Phys.: Condens. Matter* **1991**, *3*, 3215−3234.
(23) Urbach, F. The Long-Wavelength Edge of Photographic Sensitivity and of the Electronic Absorption of Solids. *Phys. Rev.* **1953**, *92*, 1324−1324.
(24) Venkateshvaran, D.; Nikolka, M.; Sadhanala, A.; Lemaur, V.; Zelazny, M.; Kepa, M.; Hurhangee, M.; Kronemeijer, A. J.; Pecunia, V.; Nasrallah, I.; et al. Approaching Disorder-Free Transport in High-Mobility Conjugated Polymers. *Nature* **2014**, *515*, 384−388.
(25) Kronemeijer, A. J.; Pecunia, V.; Venkateshvaran, D.; Nikolka, M.; Sadhanala, A.; Moriarty, J.; Szumilo, M.; Sirringhaus, H. Two-Dimensional Carrier Distribution in Top-Gate Polymer Field-Effect Transistors: Correlation between Width of Density of Localized States and Urbach Energy. *Adv. Mater.* **2014**, *26*, 728−733.
(26) Greiner, M. T.; Helander, M. G.; Tang, W.-M.; Wang, Z.-B.; Qiu, J.; Lu, Z.-H. Universal Energy-Level Alignment of Molecules on Metal Oxides. *Nat. Mater.* **2012**, *11*, 76−81.
(27) Hoye, R. L. Z.; Ehrler, B.; Böhm, M. L.; Muñoz-Rojas, D.; Altamimi, R. M.; Alyamani, A. Y.; Vaynzof, Y.; Sadhanala, A.; Ercolano, G.; Greenham, N. C.; et al. Improved Open- Circuit Voltage in ZnO-PbSe Quantum Dot Solar Cells by Understanding and Reducing Losses Arising from the ZnO Conduction Band Tail. *Adv. Energy Mater.* **2014**, *4*, 1301544.
(28) Kim, Y.-H.; Cho, H.; Heo, J. H.; Kim, T.-S.; Myoung, N.; Lee, C.-L.; Im, S. H.; Lee, T.-W. Multicolored Organic/Inorganic Hybrid Perovskite Light-Emitting Diodes. *Adv. Mater.* **2015**, *27*, 1248−1254.
(29) Hayer, A.; Köhler, A.; Arisi, E.; Bergenti, I.; Dediu, A.; Taliani, C.; Al-Suti, M.; Khan, M. S. Polymer Light-Emitting Diodes with Spin-Polarised Charge Injection. *Synth. Met.* **2004**, *147*, 155−158.
(30) Stranks, S. D.; Burlakov, V. M.; Leijtens, T.; Ball, J. M.; Goriely, A.; Snaith, H. J. Recombination Kinetics in Organic-Inorganic Perovskites: Excitons, Free Charge, and Subgap States. *Phys. Rev. Appl.* **2014**, *2*, 034007.
(31) Dai, X.; Zhang, Z.; Jin, Y.; Niu, Y.; Cao, H.; Liang, X.; Chen, L.; Wang, J.; Peng, X. Solution-Processed, High-Performance Light-Emitting Diodes Based on Quantum Dots. *Nature* **2014**, *515*, 96−99.
(32) Hoke, E. T.; Slotcavage, D. J.; Dohner, E. R.; Bowring, A. R.; Karunadasa, H. I.; McGehee, M. D. Reversible Photo-Induced Trap Formation in Mixed-Halide Hybrid Perovskites for Photovoltaics. *Chem. Sci.* **2015**, *6*, 613−617.
(33) Hoye, R. L. Z.; Muñoz-Rojas, D.; Musselman, K. P.; Vaynzof, Y.; MacManus-Driscoll, J. L. Synthesis and Modeling of Uniform Complex Metal Oxides by Close-Proximity Atmospheric Pressure Chemical Vapor Deposition. *ACS Appl. Mater. Interfaces* **2015**, *7*, 10684−10694.

DOI: 10.1021/acs.nanolett.5b02369
Nano Lett. 2015, 15, 6095−6101